ACS APPLIED MATERIALS & INTERFACES

www.acsami.org

Research Article

# Water-Based Hydrophobic Paints for Daytime Radiative Cooling

Abdulrahman K. Aljwirah, Xiaojie Liu, Orlando Rivera Gonzalez, Khalid Alhammadi, Won-June Lee, Ioanna Katsamba, and Xiulin Ruan*,▽

Cite This: ACS Appl. Mater. Interfaces 2025, 17, 32914−32927

Read Online

ACCESS | Metrics & More | Article Recommendations | Supporting Information

**ABSTRACT:** Radiative cooling paints and coatings make for an effective and scalable approach to implementing daytime cooling. However, paints often contain volatile organic compounds (VOCs), which pose health hazards and harm the environment. Therefore, the negative effects of VOCs must be resolved to ensure full implementation of paints as a radiative cooling technology. In this study, single-layer and metal-free, water-based and hydrophobic $BaSO_4$, $CaCO_3$, and hBN radiative cooling paints are presented. These paints demonstrate full daytime subambient cooling of 2.7, 2.6, and 2.5 °C, utilizing their high solar reflectance of 95.4, 93.7, and 96.1%, and strong sky window emissivities of 0.932, 0.924, and 0.825, for $BaSO_4$, $CaCO_3$, and hBN paints, respectively. Hydrophobic properties yield high water contact angles of 118, 139.9, and 136.7° for $BaSO_4$, $CaCO_3$, and hBN paints, respectively. The paints achieve the low VOC classification by recording 26, 18, and 30 g/L of VOC content, lower than many commercial water-based paints with VOC contents of up to 200 g/L. This work presents environmentally friendly ultrawhite radiative cooling paints, which have the potential to reduce energy costs and combat climate change.

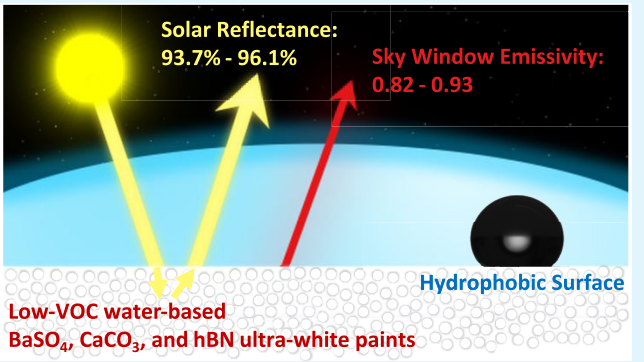


**KEYWORDS:** *daytime cooling, atmospheric sky window, water-based dispersion, low VOC, critical pigment volume concentration*



## INTRODUCTION

Air conditioners effectively cool indoor spaces, which is crucial for modern life. However, they are also energy-intensive and release heat into the outdoor ambient air, contributing to the urban heat island effect and global warming. For example, Saudi Arabia spends >70% of all its electricity on AC and cooling applications,[1] contributing to a cumulative increase in annual temperature of 1.8 °C over a 33-year period.[2] In fact, investments in AC units are expected to expand further to tailor to the urban population of many developing countries by 2050.[3] Therefore, there are pressing cooling needs for many countries, with high demands for cooling solutions that are cost-effective and environmentally responsible. Radiative cooling (also: daytime cooling) is an efficient passive technology that operates by cooling a surface below its local ambient temperature while under direct sunlight.[4−6] Radiative cooling minimizes solar heating by fully reflecting the solar irradiation within the solar spectrum (0.25−2.5 $\mu$m), which consists of the ultraviolet (UV), visible (VIS), and near-infrared (NIR) energy bands. Simultaneously, it boosts thermal emittance within the transparent atmospheric window, or "sky window", to dissipate thermal energy into deep space. Therefore, below-ambient daytime cooling can be achieved if the thermal radiation emitted surpasses the level of absorbed solar irradiation.

Initial attempts at harnessing the radiative cooling potential date back to the 1970s, where an aluminum plate was coated with titanium dioxide ($TiO_2$) commercial white paint, which successfully achieved daytime subambient cooling.[5] However, it is noteworthy that the cooling efficacy was largely influenced by the metal substrate rather than the single layer of commercial white paint. Subsequent successful iterations of full daytime subambient cooling solutions were introduced in various approaches, with photonic crystals among the earliest demonstrated concepts.[6] It still achieves some of the highest performance within the daytime cooling field with an ultrahigh reflectance of 97%. It demonstrates an excellent proof of concept, yet the high cost of multilayer nanofabrication forms a constraint for real-world scalability. Additional conceptual frameworks have been introduced such as polymer−metal and silica−metal dual layers,[7] radiative cooling with cellulose-based fibers,[8] and thermally optimized structural materials,[9] all of which demonstrate effective subambient cooling. They

Received: March 20, 2025
Revised: May 13, 2025
Accepted: May 14, 2025
Published: May 21, 2025

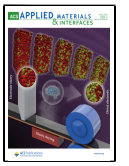

comprise innovative concepts such as multilayered polymer−metal systems and cellulose-based technologies. However, these concepts may require highly reflective and precious metals such as silver or utilize chemical processing, which often relies on solvents that produce VOCs.[10] Many of these proposed solutions face challenges in terms of their economic viability, scalability, or sustainability. A particularly interesting technology involves the use of a paint-like porous polymer coating,[11] which undergoes a phase inversion process to generate a light scattering porous structure, which facilitates daytime subambient cooling. However, this novel concept is different from the commercial particle−matrix paint format; hence, further studies may be addressed toward the maintenance of its nanopores over time. In parallel, theoretical investigations have focused on $TiO_2$-based paints to be implemented in radiative cooling paints.[12] The theoretical model employed a broad particle size distribution of $TiO_2$ to optimize the light scattering performance. Nonetheless, $TiO_2$-based formulations have a performance constrained attributed to $TiO_2$'s high solar absorption in the UV band, due to the low electronic band gap of $TiO_2$ (3.2 eV).[13−15] Nonetheless, $TiO_2$ remains the standard white pigment for most commercial paint, which is the reason that most single-layer commercial paints cannot achieve daytime cooling independently. Upon comprehensive review of the paint and coating market, high-performance metal-free and single-layer radiative cooling paints were created utilizing ultrawhite pigments.[13−15] The ultrawhite radiative cooling paints were fabricated utilizing calcium carbonate ($CaCO_3$), barium sulfate ($BaSO_4$), and hexagonal boron nitride (hBN) nanoplatelets in an acrylic matrix.[13−15] They demonstrated remarkable solar reflectance values of 95.5, 98.1, and 97.9%, along with high thermal emittance values of 0.94, 0.95, and 0.84 in the atmospheric "sky window" for $CaCO_3$, $BaSO_4$, and hBN acrylic paints, respectively.[13−15] Despite the high performance and scalability of these daytime cooling solutions, their fabrication method relies heavily on VOCs.[13−15] They utilize dimethylformamide (DMF) to dissolve the acrylic binder,[13−15] which is a toxic and flammable solvent capable of producing photochemical smog.[16,17] Therefore, VOC mitigation is essential for the successful commercialization and sustainability of ultrawhite radiative cooling paints.[18] While the paint-like porous polymer contains a low VOC mixture, the high evaporation rate and high flammability of acetone pose some safety concerns for such a coating system. Additional forms of daytime cooling paints and coatings were pursued, utilizing novel blends of the mentioned porous polymer and pigment−polymer hybrid systems.[19,20] Recently, Lio et al. developed a water-based radiative cooling paint with no VOC content utilizing hollow glass beads and the porous polymer to enable light scattering.[19] However, the performance was limited, and daytime below-ambient cooling was not achieved. Additional works of water-based radiative cooling systems were recently published using calcined kaolin[20] and polymer−glass bead blend,[21] which demonstrate good daytime cooling performance. However, the work mentioned may be limited due to utilizing a fluorocarbon-based polymer or relying on a thick coating layer to achieve daytime cooling. Moreover, radiative cooling paints should exhibit robust and durable performance, similar to most commercial paints. Paints typically can serve several functions, such as surface protection, UV stability, mechanical durability, and more. For example, water-based systems inherently contain hydrophilic groups[22] that highly affect surface wettability[23] and may result in water-related damages. To mitigate water-related defects, many surfaces utilize specialized coatings and chemical treatments to impart hydrophobicity and a nonwetting effect,[24] such as applying topcoats, or adding chemical treatments, such as fluorocarbon or silane additives within a paint's composition. Due to the use of inherently hydrophilic species, it is a prominent challenge to achieve hydrophobicity for water-based systems. Moreover, prolong exposure to different environmental conditions cause polymers to degrade and deteriorate, such as polymer oxidization, recurring mechanical abrasion, or repeated UV exposure.[25] In that regard, we attempt to bridge the gaps between novel technologies of daytime cooling, low VOC systems, and physically durable characteristics through meticulous material selection.

This work presents $BaSO_4$, $CaCO_3$, and hBN water-based cooling paints (WBCPs), which achieve full daytime cooling using metal-free and single-layer nanocomposites, with hydrophobic performance, excellent UV stability, and mechanical durability. While alternative radiative cooling pigments and fillers such as $SiO_2$,[26] $Al_2O_3$,[27] or $ZrO_2$[28] could be used, in the current work, we study the following pigments: $BaSO_4$ for some of the highest daytime cooling results, $CaCO_3$ for high performance and cost effectiveness, and hBN for high performance and lightweight features. This manuscript starts with selecting the polymer matrix along with describing fabrication and application methods. The selection process includes meeting the low VOC requirements while testing some key optical properties of the polymer matrix. Fabrication consists of a simple one-pot approach, where all of the required ingredients are homogenized before paint application. The internal structure and pigment−polymer interaction of WBCPs were then examined via scanning electron microscopy (SEM), and porosity values were calculated. After which, WBCPs' hydrophobic performance was tested via water contact angle measurements, revealing the effect of pigments' oil absorption value and pigments' surface morphology on the hydrophobic performance. Then, the low VOC status of WBCPs was confirmed, and the subambient cooling potential was tested through spectral measurements and an outdoor experiment. Additional durability parameters were then analyzed to test the performance of WBCPs in practical applications, such as testing their water resistance, material breathability, resistance to accelerated aging, and mechanical durability. This study identifies high-performance material composition with enhanced optical properties and high thermal emissivity to achieve full daytime subambient cooling. The results confirm well-designed and highly durable water-based hydrophobic daytime cooling paints. The results presented in this work were included in a provisional patent filed on November 30, 2022 and a nonprovisional international patent application (PCT/US2023/081605) filed on November 29, 2023.[29]

## RESULTS AND DISCUSSION

**WBCPs' Binder Selection.** The selection of binder−matrix components was centered on mitigating the environmental impacts of VOC emissions through eliminating the need to dissolve the polymer particles in hazardous solvents. Instead, green solvents such as water could substitute the conventional hydrocarbon solvents in paint fabrication. However, water-soluble polymers such as poly(ethylene glycol),[30] poly(vinyl alcohol),[31] or methyl cellulose[32] would not work in an outdoor setting, due to the eminent water exposure in rainy conditions.


https://doi.org/10.1021/acsami.5c05687
ACS Appl. Mater. Interfaces 2025, 17, 32914−32927

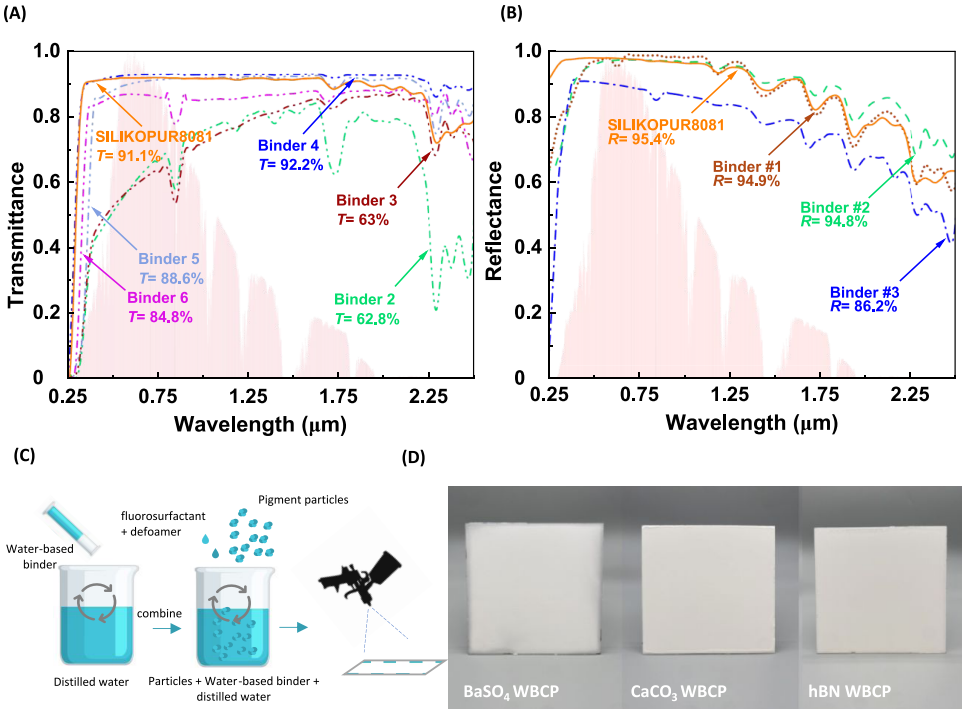


**Figure 1.** WBCP material assessments, fabrication process, and visual presentation of fabricated WBCP samples. (A) Spectral comparison of clear samples (binder only), where high transmittance is desired. SILIKOPUR8081 demonstrated high transmission across the solar region, which indicates low absorption. (B) Spectral comparison of $BaSO_4$ paints fabricated at 60% volume concentration using different water-based binders, where high solar reflectance is desired. (C) Schematic of the WBCP fabrication process. (D) Example images of WBCP samples.

Instead, polymers can be supplied in the form of an aqueous dispersion (or emulsion), where a polymer is emulsified in a stable water dispersion.[33] Polymer emulsions are designed to stabilize the nonmiscible oil particles in water using emulsifiers (also known as surfactants or dispersants). As a result, multiple immiscible and discrete polymeric phases can be stabilized in a continuous aqueous phase. Hence, paints can achieve a low VOC status by utilizing water dilution for polymer emulsions, instead of relying on solvent processing. Water-based polymer dispersions may contain up to 67% of water by weight, where the rest of the dispersion includes the nonvolatile solid content.[33] As water evaporates, the curing process starts with the fine particles of the polymer undergoing a coalescence process, which forms a cohesive film of polymeric materials. Besides minimizing VOCs, mitigating solar absorption and exhibiting high solar transmission are vital for polymers to achieve effective daytime cooling. While many water-based binders can be used for fabricating WBCPs, the overall durability and integrity of the system are just as important as its high cooling performance. Therefore, silicone-modified binders were chosen due to silicone's UV and thermal stability, mechanical flexibility, and exceptional hydrophobicity.[34] In that regard, we tested multiple water-based binders through optical spectroscopy to assess their spectral reflectance and transmittance. Spectral transmittance was tested by examining visibly clear samples (binder only), and spectral reflectance was examined by testing $BaSO_4$ paints made from these multiple water-based binders. All tested samples were applied on glass slides to obtain a substrate-independent optical performance. Among those tested binders, SILIKOPUR8081 stood out for its exceptional performance, which is a silicone-modified polyurethane water-based dispersion. The spectral transmittance of the clear samples is presented in Figure 1A, where binders with the highest solar transmittance are desired. SILIKOPUR8081's transmission was among the highest, indicating minimal solar absorption and UV stability. Similarly, Figure 1B shows the spectral reflectance of $BaSO_4$ paints made from different water-based binders, where SILIKOPUR8081 recorded the highest solar reflectance. As a result, SILIKOPUR8081 was chosen to be the WBCPs' binder throughout this work.

**Paint Fabrication.** This work utilized binder-to-pigment relationships to formulate high-performance WBCPs. The fabrication process is compatible with industrial manufacturing processes, where pigments and binders are stabilized in one solution using a carrier (i.e., solvent). WBCPs employed high pigment volume concentration (PVC) to boost light scattering in the solar wavelength.[35] While pigments typically have their critical volume concentration (cPVC) between 30% and 60%, increasing the PVC beyond the cPVC limit leads to a steep increase in a coating's porosity (air voids).[36,37] Interestingly, an air pore can act as a scattering particle when having a feature size comparable to the peak wavelength of solar irradiation (~500 nm), which can enhance the overall scattering of a coating.[38] The ASTM D281[39] test was performed on each pigment type to obtain its oil absorption value, which is a value that determines the amount of oil needed to wet the surface area of a pigment and to fill voids between the pigment particles.[40] Therefore, pigments' oil absorption values were determined to assess each pigment's cPVC value. Measured oil absorption values demonstrate wide deviation between the used pigments, such as 20 g of oil/100 g of $BaSO_4$, 80 g of oil/100 g of $CaCO_3$, and 96 g of oil/100 g of hBN. These oil absorption values yield calculated cPVC values of 50%, 30%, and 31% for $BaSO_4$, $CaCO_3$, and hBN, respectively. Hence, WBCPs employed a high PVC of 60% to induce porosity


https://doi.org/10.1021/acsami.5c05687
ACS Appl. Mater. Interfaces 2025, 17, 32914−32927

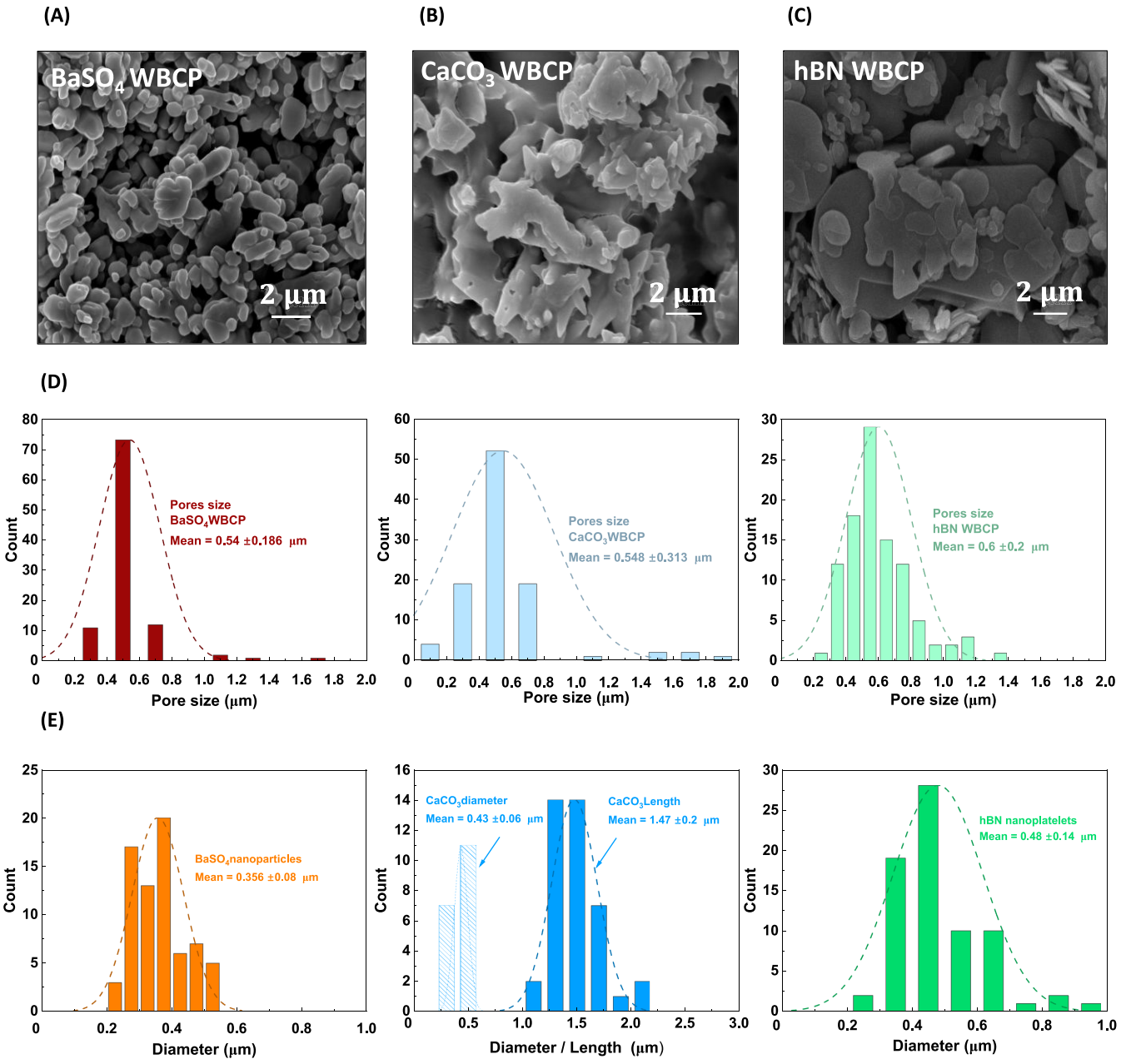


**Figure 2.** SEM characterization of WBCPs. (A) Top-view SEM image of the $BaSO_4$ paint showing its spherical nanoparticles. (B) Top view SEM image of the $CaCO_3$ paint showing its needle-like particles. (C) Top view SEM image of the hBN paint showing its platelet-shaped nanoparticles. (D) Pore size distribution, which shows the mean pore size values for each paint configuration. The variation of pore size may be affected by the particles' morphology and random packing, where higher porosity and variation in pore size may be obtained. (E) Particle size distributions for each paint configuration. It shows the means and standard deviations of the $BaSO_4$ particle diameter size, $CaCO_3$ particle length and diameter sizes, and hBN platelet diameter size. The results show a particle size distribution of $BaSO_4$ nanoparticles, $CaCO_3$ particles, and hBN nanoplatelets aligned with the solar wavelength, which indicates their effective light scattering.

formation and boost the overall light scattering, which is a common practice for radiative cooling solutions.[41,42] A detailed explanation on measuring the oil absorption and cPVC calculations is presented in Supporting Information Note 1. Furthermore, Figure 1C illustrates the fabrication process of WBCPs, which starts by mixing a water-based binder in distilled water for 30 min, followed by mixing the pigment for an additional hour. An anionic fluoro-surfactant was added to lower the overall interfacial surface tension of the paint solution,[43] which can improve substrate wetting. Also, an antifoaming agent was used to eliminate bubble formation under high agitation during paint fabrication. The antifoaming agent contains silica nanoparticles that can act as active bubble breakers to effectively eliminate foaming.[44] Both the antifoaming agent and the fluoro-surfactant are labeled as solvent/VOC-free solutions and were added at 0.1%−0.3% by weight. These additives, however, proved to be supplementary components rather than essential constituents, as they had no significant effect on the cooling performance. The fineness of grind of WBCPs was tested via ASTM D1210[45] to ensure complete dispersion of pigments. Then, WBCPs are spray-coated onto glass slides or aluminum plates using a spray gun


https://doi.org/10.1021/acsami.5c05687
ACS Appl. Mater. Interfaces 2025, 17, 32914−32927

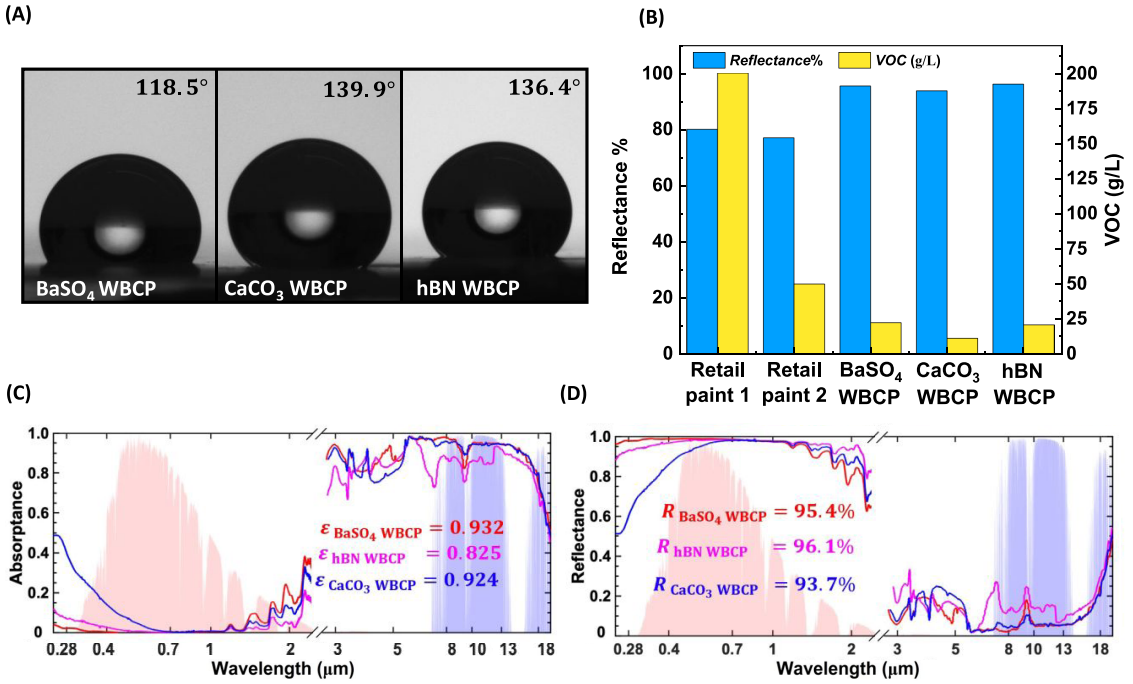


**Figure 3.** Hydrophobic performance, VOC classification, and optical and thermal characterization of WBCPs. (A) Hydrophobic test was obtained by placing a sessile droplet over the WBCPs to show WBCPs' hydrophobic capabilities by measuring their water contact angles. (B) A comparison of reflectance versus VOC content of the paint was done between water-based commercial white paints and WBCPs. WBCPs exhibit higher reflectance and lower VOC content compared to water-based commercial white paints. (C) Spectral absorption of WBCPs, where it recorded low absorption in the solar region (0.25−2.5 $\mu$m) and high absorption in the sky window region (8−13 $\mu$m). (D) Spectral reflectance of WBCPs, where it recorded high solar reflectance in the solar region and low reflectance in the sky window region.

with a 1.4 mm nozzle at an operating pressure of 3.5 bar. The fabricated paint samples are left to dry under ambient conditions, producing ultrawhite, opaque, and hydrophobic surface characteristics. A visual presentation of WBCP samples that were tested in this study is presented in Figure 1D.

**SEM Characterization.** During WBCP curing, pigment and polymer particles can spontaneously arrange into hierarchical structures that are influenced by pigments' morphologies, densities, and shear forces.[46] Moreover, the pigment's oil absorption value has shown the ability to promote or reduce pigment−matrix interactions, which consequently influence the wettability of the paint. The SEM images of WBCPs reveal pigments' morphologies, pigment−polymer interactions, and pore formation, as shown in Figure 2A−C. The SEM image of the fabricated $BaSO_4$ paint is shown in Figure 2A, where a clear distinction between the oil phase (binder) and the pigment phase ($BaSO_4$ particles) is noticed. The binder phase is depicted as irregular fragments of particles, where the $BaSO_4$ phase is identified by its spherical morphology. It is seen that the low oil absorption value of $BaSO_4$ inhibits efficient pigment−matrix blending; thus, $BaSO_4$ particles remain exposed to the atmosphere instead of complete encapsulation by the binder. Similarly, Figure 2B illustrates the SEM images of the $CaCO_3$ paint, which shows a significant improvement in pigment−matrix interaction, where $CaCO_3$ particles are fused within the polymer matrix. This indicates strong cohesive bonding and highlights the role of $CaCO_3$'s oil absorption value in promoting pigment−matrix contact. The image features the scalenohedral morphology (ellipsoidal shape) of $CaCO_3$ and the hierarchical porous network of the paint. Likewise, Figure 2C exhibits the SEM image of hBN paint, which clearly shows the randomly oriented hBN nanoplatelets and the paint's porous structure. It also exhibits the binder's planar orientation, which we believe is warped due to the interaction with hBN nanoplatelets. Formation of pores within these paints also confirms the WBCPs' design in adopting PVC > cPVC, where porosity content was calculated to be 32%, 54%, and 62% for $BaSO_4$, $CaCO_3$, and hBN WBCPs, respectively. Note that the final pigment volume concentration of WBCPs changes as air voids are introduced to form multiphase nanocomposites. Consequently, WBCPs form pigment/binder/air pores volumetric ratios of 40.8%:27.2%:32% for $BaSO_4$, 27%:18%:55% for $CaCO_3$, and 22.4%:14.9%:62.7% for hBN WBCPs. The results indicate that the large aspect ratio of the pigment and the large deviation between PVC and cPVC lead to higher porosity such as in $CaCO_3$ and hBN paints' porosity content. Additional SEM analysis was conducted to obtain the air pores and particle size distributions of WBCPs.

Figure 2D exhibits the pore size distribution of WBCPs, all of which form pores that are aligned with the solar wavelength. Similarly, Figure 2E exhibits the particle size distribution of ultrawhite pigments. It features the average diameter of $BaSO_4$, the average length and diameter of $CaCO_3$, and the average diameter of hBN nanoplatelets, all of which are aligned with the peak solar wavelength. As indicated in recent modeling,[47] strong sunlight scattering requires the mean particle size to be around the peak solar wavelength, while it is not sensitive to size uniformity. Hence, nonuniform size can be preferred in practical applications, instead of using single particle size materials. Due to the high alignment of pores and particle sizes to the peak solar wavelength, WBCPs are expected to demonstrate strong light scattering performance and high potential for daytime cooling. Additional SEM images are


https://doi.org/10.1021/acsami.5c05687
ACS Appl. Mater. Interfaces 2025, 17, 32914−32927

provided in Figures S1, S2, and S3, which exhibit the fluorosurfactant particles and antifoaming silica nanoparticles.

**Hydrophobicity Characterization.** As noted, paints and coatings should serve multipurpose functions, one of which is surface protection against water contamination, which can be more challenging for water-based systems. As mentioned, hydrophobicity can be achieved through chemical modification, using water-repellent compounds such as fluorocarbons or silanes.[48,49] Such hydrophobic agents are used to diminish the surface free energy of the material and impart water-repelling and nonwetting characteristics. For example, fluorocarbons form robust carbon−fluorine bonds, effectively precluding interactions with other compounds, such as oils and water. However, fluorocarbon compounds pose a major environmental concern due to their contribution to pollution and their toxicity.[50] On the other hand, polysiloxane compounds commonly feature nonpolar alkyl chains at the solid−air interface, which limits the hydrogen bonding with water molecules.[51] Therefore, silicone compounds can lower the surface free energy and impart hydrophobicity as a low-toxicity alternative to fluorocarbons. Furthermore, surface roughness also plays an important role in enhancing hydrophobicity and is crucial for achieving superhydrophobic surfaces.[52] In this study, WBCPs' hydrophobicity was achieved by utilizing a silicone-modified water-based binder and was examined by water contact angle measurements, implementing the sessile droplet method. The contact angle was measured as the angle formed (in this case by a water droplet) at the three-phase contact line (the junction where the solid, liquid, and vapor phases meet). After several days of curing, paint samples were tested under ambient conditions, with no special drying or additional surface treatments of the paint samples. The aim was to achieve reproducible and predictable hydrophobic performance with no external influence on the paint samples. A 10 $\mu$L water droplet is carefully placed onto the paint surface until it reaches a sessile state (when the three-phase boundary line is not moving). Then, an image of the droplet is taken to accurately determine the contact angle. Contact angle measurements obtained 118.5, 139.9, and 136.4° for $BaSO_4$, $CaCO_3$, and hBN WBCPs, respectively, as shown in Figure 3A. While all WBCPs are made from the same silicone-modified water-based binder, there is a clear difference in their hydrophobic performance. Such an obvious distinction could be linked to pigments' surface morphology and oil absorption values. Pigments with a higher aspect ratio can enhance surface roughness, while higher oil absorption can limit polar interactions and inhibit hydrogen bonding. Both effects are expected to boost the hydrophobic performance of a composite. These deductions align with higher oil absorption values and higher aspect ratio morphologies of $CaCO_3$ and hBN. This also correlates with the low oil absorption value and highly symmetric spherical morphology of $BaSO_4$. Additional SEM images are included in Figure S4, highlighting the varying surface roughness of WBCPs. Note that a complete study on WBCP wettability hysteresis is beyond the scope of this work and can be addressed in a future work.

**WBCPs' VOC Content.** As noted, most VOCs pose major health and environmental hazards; hence, it is desirable to mitigate such negative effects for daytime cooling paints. We identified the VOC content of the WBCPs based on the guidelines of the South Coast Air Quality Management District (AQMD)[53]

$$\mathrm{VOC}_{\mathrm{WBCPs}} = \left( \frac{m_{\mathrm{total}} - m_{\mathrm{H_2O}} - m_{\mathrm{solids}}}{V_{\mathrm{measured}}} \right) \quad (1)$$

where $m$ stands for the mass of each component in the paint mixture, and $V$ represents the measured volume of paint solution. The WBCPs contain 26 g/L, 18 g/L, and 30 g/L of VOC content for $BaSO_4$, $CaCO_3$, and hBN paints, respectively. These results are well below the mandated levels of 50 g/L based on the South Coast Air Quality Management District Rule 113 (Feb 2016).[54] Paints and coatings with VOC levels below the mandated levels achieve the low VOC status, which is much lower than the VOC compliant status.[55] For example, some commercially available interior and exterior water-based paints can have a VOC compliance status with VOC levels of up to 100 g/L, which is way above the low VOC limit.[56] A comparison between our WBCPs and commercial water-based white paints is shown in Figure 3B, which compares their total solar reflectance versus the VOC content of the paints. It highlights how WBCPs achieve high total solar reflectance while also achieving low VOC levels. On the other hand, commercial water-based white paints demonstrate moderate solar reflectance and VOC content of up to 200 g/L. These results indicate that high potential for daytime subambient cooling can be achieved via low-VOC water-based paint systems and that cooling performance is not exclusive to solvent-based paints. Further comparisons between WBCPs and water-based commercial white paints are included in Figure S5A, where the solar reflectance versus paint's thickness is shown, and in Figure S5B, where the spectral reflectance was analyzed.

**Evaluating the Radiative Cooling Performance.** Next, the spectral response in solar and mid-IR regions was measured to evaluate WBCPs' daytime cooling performance. Figure 3C showcases WBCPs' strong thermal emittance within the sky window region (8−13 $\mu$m), and Figure 3D displays WBCPs' high solar reflectance within the UV−vis−NIR regions (0.25−2.5 $\mu$m). Spectral reflectance features negligible UV absorption facilitated by the high-band-gap pigments, while the selected *PVC* facilitates efficient scattering within the NIR region. Figure S6 presents WBCPs' measured solar reflectance and predicted solar reflectance utilizing Mie theory[57] as a function of paints' thickness. Furthermore, the potential of demonstrating fall daytime subambient cooling of materials can be evaluated using the established radiative cooling figure of merit[13] defined as

$$\mathrm{RC} = \varepsilon_{\mathrm{sky}} - r(1 - R_{\mathrm{solar}}) \quad (2)$$

where $\varepsilon_{\mathrm{sky}}$ represents the sky window emissivity, $R_{\mathrm{solar}}$ signifies the total solar reflectance, and $r$ denotes the ratio of the incident solar irradiance of 1000 W/m$^2$ to the blackbody's emissive power within the sky window of 140 W/m$^2$, so $r$ is approximately 7.14. This allowed us to calculate the net radiative cooling power. According to this framework, an increase of 0.01 in solar reflectance equates to an enhancement of 0.0714 in sky window emissivity regarding the cooling performance. This metric reveals that cooling below the surrounding temperature is theoretically feasible when the RC value is above zero. Note that RC is obtained to fairly evaluate the cooling performance independently of weather conditions. Standard RC metrics for $BaSO_4$, $CaCO_3$, and hBN paints were 0.603, 0.474, and 0.546, respectively, confirming WBCPs' full daytime subambient cooling capability. To further validate the


https://doi.org/10.1021/acsami.5c05687
ACS Appl. Mater. Interfaces 2025, 17, 32914−32927

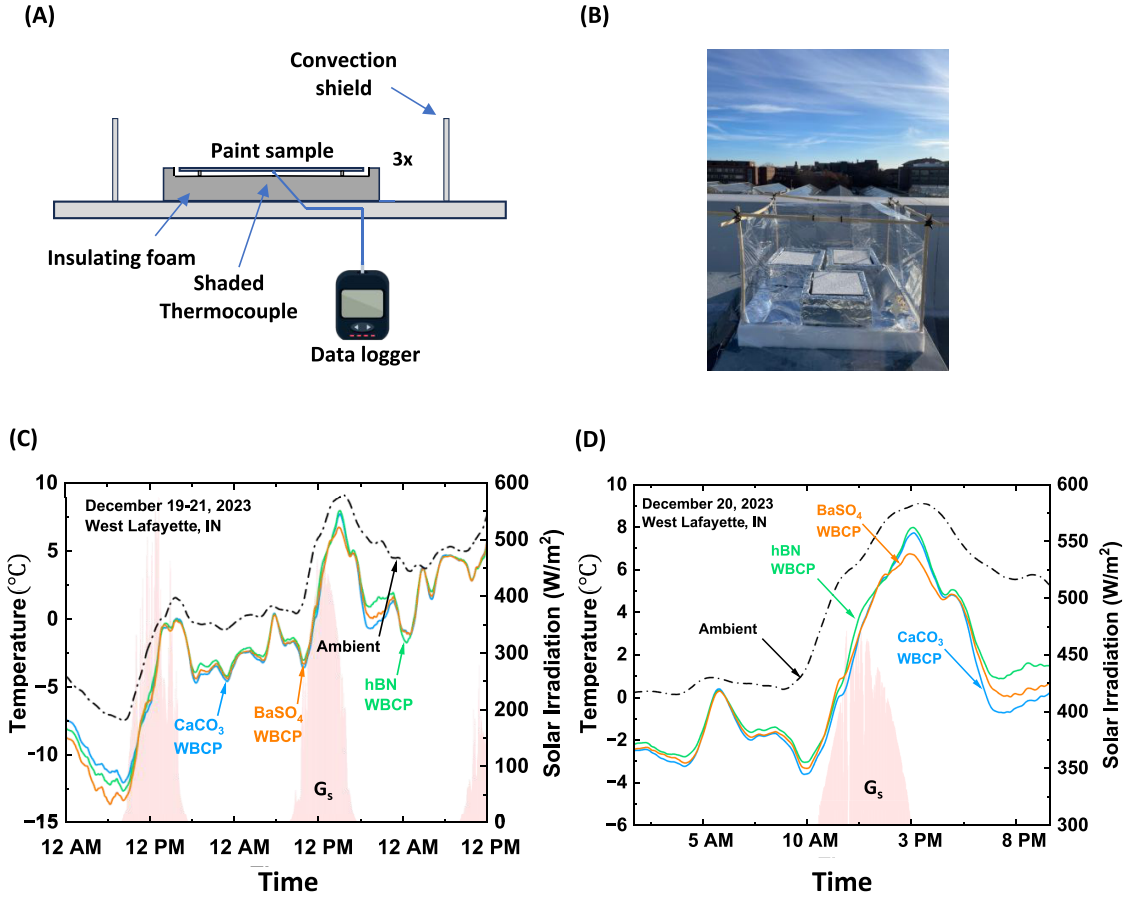


**Figure 4.** Experimental apparatus and cooling performance of WBCPs. (A) Schematic of the field test where samples were applied on a 0.6 mm thick 6 in. × 6 in. aluminum plate. The paint samples were suspended above a Styrofoam insulating base to minimize conductive ground heating. Samples were shielded by a transparent PE film to minimize forced convection. Ambient temperature and solar irradiation data were obtained from a local weather station. (B) An image of the tested WBCP samples, which were suspended and shielded to minimize conductive and convective parasitic heating. (C) Continuous subambient cooling of WBCP samples over a 60 h period of the outdoor test. (D) Magnified section of the outdoor test showcasing the cooling performance under the solar peak on December 20, 2023.

RC metrics, an experimental setup was used that confirms the subambient cooling ability of WBCPs, which relied on monitoring the ambient and paints' temperatures, as shown in Figure 4A. Each paint sample was applied to 6 in. × 6 in. aluminum plates, with paint thicknesses of approximately 400 ± 46, 550 ± 46, and 200 ± 65 $\mu$m for $BaSO_4$, $CaCO_3$, and hBN paint samples, respectively. These thicknesses are sufficiently large as validated in Figure S6, where solar reflectance saturates to 95.4% for $BaSO_4$, 94.1% for $CaCO_3$, and 96.3% for hBN WBCPs. $T_{ambient}$ was obtained from a local weather station, while $T_{WBCPs}$ was monitored by using T-type thermocouples attached to the backside of each paint sample. The tested samples were suspended in a Styrofoam insulating base to reduce the conductive heat transfer. Also, the samples' enclosure was encased by a transparent polyethylene film to mitigate parasitic thermal losses via convective energy transfer. The experimental testing setup is shown in Figure 4B, and it was performed on December 19−21, 2023, in West Lafayette, IN. The cooling efficacy of WBCPs was validated by maintaining continuous daytime subambient cooling, as shown in Figure 4C. For this duration, ambient temperatures varied between ∼10 °C and −7.5 °C, with $BaSO_4$, $CaCO_3$, and hBN WBCPs averaging 3.3 °C, 3.1 °C, and 2.9 °C below ambient, respectively. Separating daytime and nighttime, these numbers were 2.7 °C, 2.6 °C, and 2.5 °C below ambient for $BaSO_4$, $CaCO_3$, and hBN WBCPs, respectively, during daytime and 3.75 °C, 3.3 °C, and 3.3 °C below ambient for $BaSO_4$, $CaCO_3$, and hBN WBCPs, respectively, during nighttime. This validates both the cooling performance of WBCPs in achieving subambient temperatures and confirms RC as a reliable metric for evaluating radiative cooling materials.

Figure 4D exhibits an enlarged portion of the outdoor test, where a clear below-ambient cooling is shown under peak solar irradiation of 444 $W/m^2$, recorded on December 20, 2023, in West Lafayette, IN. The cooling performance with respect to relative humidity and wind speed are is presented in Figure S7A,B. Additional analysis included WBCPs' cooling power in $W/m^2$ is presented in Supporting Information Note 9 and Figure S8. Table 1 reports previously reported daytime cooling materials with comparable cooling performance to that of WBCPs.

**Durability and Reliability Test Results.** It is imperative to acknowledge that coatings must meet sufficient durability requirements, such as cohesion, adhesion, color retention, and resistance to the overall degradation of polymers. It is known that paints and coatings are often susceptible to degradation due to various weather conditions including water-induced damage.[58] Such damage occurs due to water absorption and contamination within the paint's film. When water is trapped within a coating system, water vapor molecules cause a


https://doi.org/10.1021/acsami.5c05687
ACS Appl. Mater. Interfaces 2025, 17, 32914−32927

**Table 1. Summary and Comparison of the Proposed WBCPs and Previous Radiative Cooling Materials in the Literature**

| material type | thickness ($\mu$m) | total solar reflectance (%) | sky window emissivity | RC |
|---|---|---|---|---|
| $BaSO_4$ paint (this work) | ~400 | 95.4 | 0.932 | 0.603 |
| $CaCO_3$ paint (this work) | ~400 | 93.7 | 0.924 | 0.474 |
| hBN paint (this work) | ~150 | 96.1 | 0.825 | 0.546 |
| cellulose-based composite[8] | 700 | 93 | 0.92 | 0.42 |
| radiative cooling structural material[9] | -- | 96 | $0.9 < \varepsilon_{(8-13)\ \mu m}$ | 0.614 |
| porous polymeric coating[11] | 300 | 96 | 0.97 | 0.547 |
| $CaCO_3$–acrylic paint[13] | 400 | 95.5 | 0.94 | 0.62 |
| $BaSO_4$–acrylic paint[14] | 400 | 98.1 | 0.95 | 0.77 |
| hBN–acrylic paint[15] | 150 | 97.9 | 0.83 | 0.612 |

pressure build-up at the substrate–coating interface. As the interfacial pressure increases, surface anomalies such as blistering, cracking, or disintegration of a coating can occur, resulting in a complete system failure.[59] Thus, it is essential to reduce water capillary uptake to mitigate damage related to water absorption. Water absorption is evaluated by the $W_{24}$ value, which tests surfaces' resistance to water contact over a period of 24 h following ASTM D570[60] guidelines. More information about the procedure of measuring the $W_{24}$ values is presented in the experimental procedures section.

WBCPs showed minimal water uptake as noticed in Figure 5A, where $W_{24}$ values <0.1 kg/($m^2$ $h^{0.5}$) indicate low water absorption. Notably, hBN and $CaCO_3$ paint samples exhibit even lower $W_{24}$ values than the $BaSO_4$ paint, underscoring their higher hydrophobicity, as noticed.

Furthermore, many polymers typically experience degradation, depending on the nature of their chemical bonds. These materials are vulnerable to UV exposure that can break down their molecular bonds.[61,62] In particular, UV absorption in paints and coatings often leads to surface anomalies such as yellowing, cracking, and overall material degradation.[63] Therefore, it is essential that paints and coatings can withstand such harsh exposure in order to maintain their high performance over time. To validate the integrity of WBCPs, they underwent accelerated aging tests for 100, 200, and 250 h, based on ISO 11341[64] artificial weathering standards for varnishes and paints. During the tests, WBCPs were subjected to continuous UV irradiation, heat, and humidity cycles to replicate long-term outdoor conditions in a shorter time frame. After testing, WBCPs were examined for any possible decay in solar reflectance, loss of hue, lightness, or color stability. While some polymeric coatings can experience a color change in a shorter time frame,[65,66] our WBCPs experienced a negligible change in solar reflectance even after 250 h of aging, as shown in Figure 5B. This stability is attributed to both the inherent UV stability of silicone-based binders, which are known for their robust Si–O backbone and to the incorporation of high-band-gap materials that effectively reflect UV radiation. Moreover, it is vital that coatings achieve high breathability, as it allows for the release of any trapped water vapor from the substrate to the environment. Therefore, breathable paints can eliminate any pressure build-up between the paint layer and the substrate and can maintain reliable mechanical adhesion. High breathability can also be related to fast drying, as moisture in water efficiently breaks away from the internal structure of a coating. To evaluate its breathability, WBCP samples were submerged for 1 h and then left to dry for 1 h at ambient conditions. The WBCP samples were weighed at every step, where negligible mass difference at dry and redry stages is shown in Figure 5C, which confirms the high water vapor permeability of WBCPs. An additional abrasion resistance test was implemented to evaluate the paints' ability to withstand repeated wear exerted by abrasive materials. The ASTM D4060[67] Taber Abraser standardized test was implemented over 2500 cycles of wear, where mass loss was documented every 250 cycles. A pair of CS-10 abrasive wheels were used, each exerting a weight force of 2.45 N, which were resurfaced every 500 cycles. The WBCPs achieved an abrasion resistance that is comparable to commercial products and the previous acrylic-based formulations, as shown in Figure 5D. Notably, $BaSO_4$ paint recorded the highest mass loss among the fabricated paints, which may be related to its lower oil absorption value, affecting the pigment–matrix interactions. Furthermore, mechanical adhesion is a key characteristic of paints, achieved by chemical bonding and/or mechanical interlocking with the substrate.[68] With proper adhesion, paints can have an extended service life and can maintain a protective barrier between the substrate and the immediate environment. Loss of adhesion is determined by film delamination, which can be assessed using self-adhesive tape as per ASTMD3359.[69] The adhesion strength of WBCPs was examined by the tape test and cross-cut method, as illustrated in Figure 6A, which utilized 4 N/cm adhesive tape placed over a cross-cut pattern.

The tape is left to adhere for 90 s and then rapidly peeled with a close to 180° angle, after which loss of adhesion or surface defects are monitored, as seen in Figure 6A. Adhesion performance is classified by examining the removal of the material along the "X" cut. All WBCPs recorded a 4A rating with no visible loss, peel, or disintegration of the material, as shown in Figure 6B. The strong adhesion performance is attributed to polyurethane's strong bonding properties,[70] showcasing excellent adhesion of the paints even at high pigment content. WBCPs' strong adhesion proves that mechanical durability and effective daytime cooling can be simultaneously achieved without compromise. The sum of these tests validates the overall UV stability, water resistance, and mechanical durability of WBCPs.

## CONCLUSIONS

This work introduces metal-free and single-layer low VOC WBCPs that exhibit high solar reflectance and other highly robust characteristics such as hydrophobicity, UV stability, and mechanical durability. It successfully mitigates the toxic off-gassing of VOCs while demonstrating effective cooling and durable characteristics. High solar reflectance was achieved by utilizing high-band-gap pigments at 60% PVC content; thus, the pigments mitigate UV absorption and boost light scattering in the NIR region. Through meticulous material selection, high optical and cooling performances were experimentally shown, validating its spectral measurements and theoretical predictions. WBCPs achieved full daytime subambient cooling and outperformed other commercial products with higher solar


https://doi.org/10.1021/acsami.5c05687
ACS Appl. Mater. Interfaces 2025, 17, 32914–32927

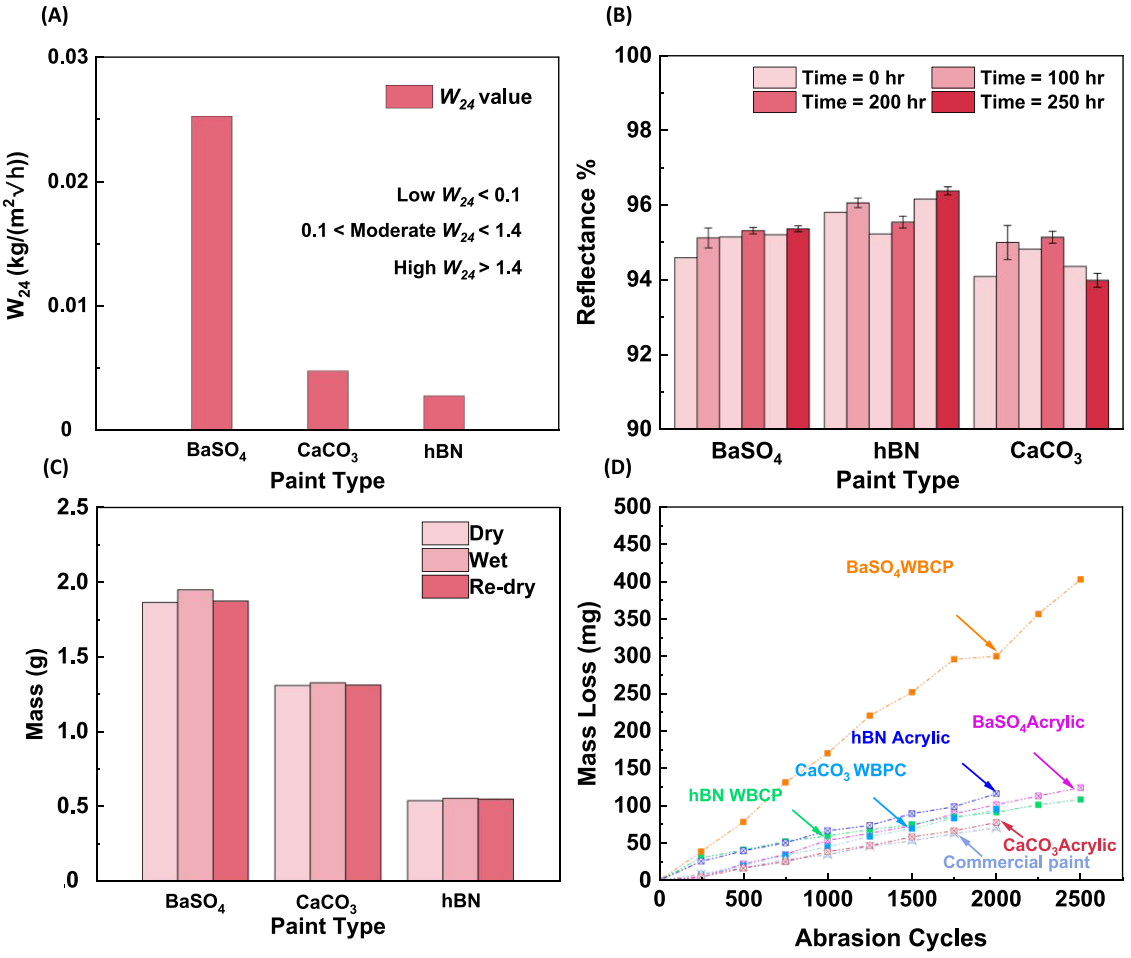


**Figure 5.** Durability of WBCPs against water absorption, accelerated aging, mechanical abrasion, and assessment of their breathability. (A) Rate of water uptake within WBCPs showing the $W_{24}$ value with the unit of $\left(\frac{\text{kg}}{\text{m}^2\sqrt{\text{h}}}\right)$. (B) Reflectance before and after accelerated aging. WBCPs' measured solar reflectance, which reveals a negligible difference before and after aging. (C) Drying capability of WBCPs, which emphasizes their high breathability and high water vapor permeability. (D) Mass loss experiment under mechanical abrasion was documented every 250 cycles. WBCPs showed mass loss comparable to those of commercial paint and previously developed acrylic paints. $BaSO_4$ paint showed a higher mass loss, which may be related to its low oil absorption value.

reflectance and lower VOC content. Despite the use of a water-based system, WBCPs produce hydrophobic surfaces with high water contact angles, low water absorption, and high water-vapor breathability. It was noticed that both oil absorption values and the surface morphology of pigments heavily influence the wetting characteristics of a hydrophobic surface. WBCPs' durability was further investigated through accelerated aging and mechanical robustness. Although excessive UV exposure was directed upon WBCPs, they experienced negligible changes in their solar reflectance, highlighting their UV stability. Additional cyclic abrasion resistance and adhesion strength tests were evaluated, demonstrating excellent mechanical durability of WBCPs. As a result, a scalable, metal-free, single-layer, environmentally friendly, hydrophobic, UV-stable, mechanically robust, with full daytime subambient cooling performance was achieved by WBCPs.

## EXPERIMENTAL PROCEDURES

**Fabrication of WBCPs.** *Materials.* $BaSO_4$ nanoparticles were purchased from Sigma-Aldrich (Reagent Plus, 99 7727−43−7). $CaCO_3$ was obtained from Atlantic Equipment Engineers CAS-Number 471−34−1. hBN nanoplatelets (SP) were acquired from Saint Gobain Advanced Ceramics, LLC. Commercial paints were tested to compare their optical performance against WBCPs. Retail paint1: Cool Wall systems Classic primer SmoothTM White 180713−123. Retail paint2: Resilience Exterior Acrylic latex K42 T 154 _ 6504−27446. A silicone-modified water-based binder (SILIKOPUR8081) and an antifoaming agent (TEGO Airex 902 W N) were supplied by EVONIK Industries. Finally, an ionic fluorosurfactant (Thetawet FS-8225) was provided by Innovative Chemical Technologies Inc (ICT).

*Fabrication Process.* First, the SILIKOPUR8081 binder is mixed with distilled water. Given the brushing method of application, WBCPs adopt an approximate binder-to-water mass ratio of 1:2 for $BaSO_4$ paint and 1:1.8 for hBN- and $CaCO_3$-based formulation. The slight difference in binder/water ratios is attributed to the difference in pigment density for each formulation and the quality of the film formation. In the spraying method of application, WBCPs implement 1:0.75 for $BaSO_4$ and hBN paints. The binder and water are mixed for 30 min using the Lab Stirrer overhead mixer with a dissolving stirrer. Next, the pigment particles are added and well mixed at high shear for 1 h, and then additives are incorporated for additional mixing. Once the solution is finely dispersed as per ASTM D1210,[45] it can then be applied via brushing or spraying onto 1 mm thick glass slides or 0.6 mm aluminum plates and cured at ambient conditions. WBCP samples' thickness values are measured via a Mitutoyo Dial Gauge Digital Plunger Type, High-Accuracy (Part number: 543−562A) with a resolution of 0.0005 mm. An average thickness value is obtained


https://doi.org/10.1021/acsami.5c05687
ACS Appl. Mater. Interfaces 2025, 17, 32914−32927

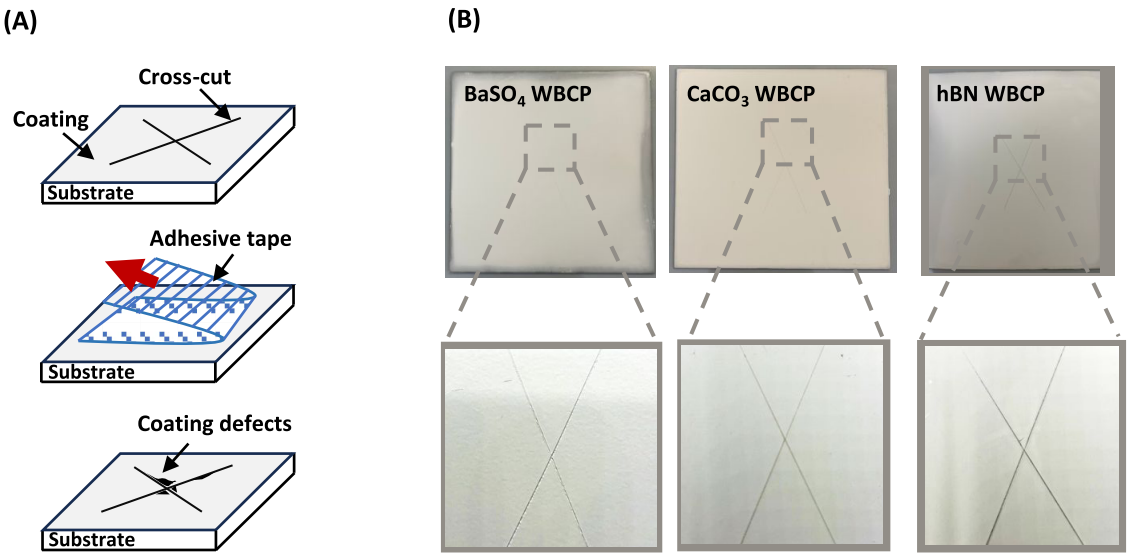


**Figure 6.** WBCPs' adhesion performance. (A) Overview of the adhesion test method. A cross pattern is cut on a coating sample, and then an adhesive tape is applied on the cross-cut pattern, after which the tape is rapidly peeled from the coating's surface to examine the adhesion strength of the paints. The adhesion strength is rated based on the amount of the paint material that is removed or peeled by the tape's pull-up force. (B) WBCPs "*x*" pattern after peeling, which shows no peel or removal of material.

using an average of five thickness readings taken within the neighborhood of the optical measurements' spots of each paint. To overcome the compression effect of the plunger, a noncompressive plastic plate is used to accurately measure the thickness. As a polymer emulsion, SILIKOPUR8081 contains volatile and nonvolatile components, where the solid mass percentage %solid is approximately 33%. The solid content is critical information to know about any polymer in an emulsion form because a paint's PVC is designed according to the solid content of a polymer. WBCPs' PVC was chosen as 60% of the solid content of SILIKOPUR8081. Pigment mass was determined by

$$m_{\text{pigment}} = \frac{m_{\text{SILKOPUR8081}} \times \%\text{solid}}{\rho_{\text{SILIKOPUR8081}}} \times \frac{\%\text{PVC}}{(1 - \%\text{PVC})} \times \rho_{\text{pigment}} \tag{3}$$

where $\rho_{\text{binder}}$ and $\rho_{\text{pigment}}$ represent the densities of the binder and pigment, respectively, while $m_{\text{pigment}}$ and $m_{\text{binder}}$ present the masses of the pigment and binder, respectively. %PVC is chosen as 60%, where (1 − %PVC) exhibits the volume concentration of the binder.

Moreover, bubbles may form due to high agitation, hence Airex 902 (solvent-free antifoamer) is added to prevent the foaming of paint. A VOC-free anionic fluorosurfactant is added to lower the surface tension of the paint mixture, which can improve the wetting of various surfaces. The addition of Thetawet FS-8225 improves surface quality, and Airex 902 facilitates an easier fabrication process. The mass of anionic fluorosurfactants (Thetawet FS-8225) and antifoamer (TEGO Airex 902 W N) is determined based on 0.1%−0.3% of total weight using

$$m_{\text{defoamer/surfactant}} = (m_{\text{SILIKOPUR8081}} + m_{\text{water}} + m_{\text{pigment}}) \times \%w \tag{4}$$

Note that neither the antifoamer nor the fluorosurfactant was counted in determining the VOC content, due to their trivial amount and being zero-VOC/solvent-free substances.

**Porosity Measurements.** The porosity of WBCPs $\varphi$ was obtained by

$$\varphi = \left(1 - \frac{V_{\text{solid}}}{V_{\text{total}}}\right) \tag{5}$$

where $V_{\text{total}}$ exhibits the physical volume of thickness multiplied by the cross-sectional area, and $V_{\text{solid}}$ presents the predicted total volume using measured mass divided by calculated density. Six specimens were evaluated for each paint configuration. The thickness of the dried paint was evaluated as an average of 5 reading measurements across the paint sample, and all fabricated samples had a 3 sq in surface area. The calculated solid density was deduced by considering the respective densities of the binder and pigment components, each weighted by their volume fractions within the mixture. Specifically, 60% of the pigment density (4.5 g/mL for $BaSO_4$, 2.71 g/mL for $CaCO_3$, and 2.1 g/mL for hBN) was combined with 40% of the solid binder density, which was estimated as 1.105 g/mL. Thus, porosity values obtained are 32%, 62.7%, and 55% with standard deviations of 2.85%, 3.2%, and 4.15% for $BaSO_4$, hBN, and $CaCO_3$ WBCPs, respectively.

**Volatile Organic Compound Calculations.** The VOC content of WBCPs was obtained using the guidelines of the South Coast Air Quality Management District (AQMD)[53]

$$\text{VOC}_{\text{WBCPs}} = \left(\frac{m_{\text{total}} - m_{\text{H}_2\text{O}} - m_{\text{solids}}}{V_{\text{measured}}}\right) \tag{6}$$

where $m$ represents the mass of each component in the paint solution and $V$ refers to the measured volume of the paint solution. The VOC content of paints is usually presented in g/L,[53] where the obtained VOC contents are approximately 26 g/L, 18 g/L, and 30 g/L for $BaSO_4$, $CaCO_3$, and hBN WBCPs, respectively. Therefore, this work achieves the low VOC status by the South Coast Air Quality Management District Rule 113 (Feb 2016) of <50 g/L.[54]

**Cooling Power Calculations.** A theoretical framework was used to assess the net cooling power of the WBCPs when subjected to solar irradiation, heat exchange with the atmosphere, and convective heat transfer. Within the scope of this model, we assume that the paint samples experience no conductive heat losses due to the insulating base. Consequently, the cooling power of the WBCPs is governed by the following equation

$$P_{\text{cooling}} = P_{\text{s}} - P_{\text{atm}} - P_{\text{solar}} - P_{\text{non-rad}} \tag{7}$$

where $P_{\text{s}}$ is the emitted heat by a paint sample as stated by Planck's law for the continuous heat emission of any terrestrial body above zero Kelvin. $P_{\text{atm}}$ is the diffuse atmospheric thermal radiation. $P_{\text{solar}}$ is the incident solar intensity term that accounts for the absorbed solar energy by the cooler. The $P_{\text{non-rad}}$ term accounts for parasitic heat transfer induced by convection and conduction. More details are included in Supporting Information Note 9.


https://doi.org/10.1021/acsami.5c05687
ACS Appl. Mater. Interfaces 2025, 17, 32914−32927

**Spectral Characterization.** Fabricated paint samples were applied on a 1 mm glass substrate to ensure high solar reflectance with substrate independence during the optical spectroscopy measurements. The solar reflectance was evaluated by using a Lambda 950 UV−VIS-NIR spectrophotometer from PerkinElmer, equipped with an integrating sphere, and calibrated by using a Spectralon diffuse reflectance reference. The total solar reflectance was obtained based on the AM 1.5 solar spectrum and reflectance reference standards. Infrared spectroscopy was evaluated using a Nicolet iS50 FTIR spectrometer accompanied by an integrating sphere from PIKE Technologies, with the reflectance standard presenting an uncertainty of ±0.02. IR measurements were conducted on a 0.6 mm aluminum plate to minimize the substrate contribution to emissivity. Spectral reflectance and transmittance were measured by utilizing the spectrometers mentioned, and spectral absorptance was calculated as follows.

$$\alpha_\lambda = 1 - \rho_\lambda - \tau_\lambda \tag{8}$$

Sky window emissivity was obtained by weighing the spectral absorptance within the 8−13 $\mu$m range by the blackbody emissive power at 300 K.

**Hydrophobic Performance Evaluation.** The wettability performance of the WBCPs was determined by examining the static contact angle of a sessile water droplet. The contact angle is defined as the angle that a liquid makes at the three-phase contact line (at the solid, liquid, and gas phases interface). A 290 Ramé-Hart Goniometer was used for the water contact angle measurements. A 10 $\mu$L water droplet was gently placed on the painted surface, allowing it to settle naturally. Then, a profile photograph of the droplet was captured to ascertain the contact angle.

**Field Test for Evaluating the Cooling Performance.** The cooling performance of WBCPs was evaluated by monitoring the paint sample's temperature and ambient temperature. The experiment was conducted on December 19−21, 2023, in West Lafayette, IN (40.4237° N, 86.9212° W). The WBCP samples were applied on 6 in. × 6 in. aluminum plates. Then, two T-type thermocouples were attached to the bottom side of the painted aluminum plates that are suspended in a Styrofoam insulating base. The paint samples were placed in an enclosure that was shielded with a transparent polyethylene film to mitigate convection losses. Local ambient temperature and solar intensity data were obtained from a local weather station.

**Durability and Longevity Characterization.** *Water Absorption and Water Vapor Permeability.* Water absorption tests were conducted using ASTM D570[60] guidelines to obtain $W_{24}$ values, which indicated the amount of absorbed water content via capillary action within a bulk material over a period of 24 h. First, the samples were weighed at the dry stage. Then, they were immersed in water for 1 h and weighed again. Subsequently, the samples were allowed to dry for 1 h at ambient conditions and weighed one more time to assess their water absorption and breathability. The $W_{24}$ values obtained on our WBCPs show a low water absorption classification. Upon drying, the paint samples nearly expelled all water content, demonstrating their high water vapor breathability.

*Weathering Exposure and Aging Characterization.* An extensive aging test was performed according to ISO 11341[64] -Varnishes and Paints, Artificial Climate, and Radiation Tests to the WBCP samples. The paint samples were placed in a Q-SUN XE-3-HC type Solar Radiation Simulator chamber with xenon lamps equipped with optical filters for 100, 200, and 250, with UV light irradiation (with a wavelength of 320−360 nm).

*Taber Abraser test.* Abrasion tests were conducted using a Taber Abraser Research Model and performed following ASTM D4060[67] guidelines. A pair of CS-10 abrasive wheels were used to wear the WBCP samples, each subjected to a force of 250*g*. The sample weights were recorded every 250 cycles to determine the mass loss, and the abrasive wheels were resurfaced every 500 cycles. The mass loss was monitored across an expanse of 2500 cycles in total, with mass loss comparable to commercially available products and previous acrylic-based paint formulations.[13−15] The abrasion resistance results are presented in Figure 5D in the Results and Discussion section.

*Adhesion Test.* The test was adopted to assess WBCPs' adhesion by applying and removing adhesive tape over cuts made on a coating film that can be applied on a metallic substrate. The WBCP samples were applied on aluminum plates, and the cross-cut adhesion tape method was utilized, which is recommended for films ≥125 $\mu$m. The test was conducted using a 4 N/cm tape, where the tape was applied on the paint's surface for 90 s and then rapidly peeled with a close to 180° angle, trying to unbind WBCPs' films. Then, the WBCPs' surfaces were visually examined for any trace of peeling, delamination, or material loss. The paint samples showed only a trace of material loss along the cross-cut, which demonstrated excellent adhesion and strong bonding of the 4A rating.

## ■ ASSOCIATED CONTENT

### Data Availability Statement

The data supporting the findings of this study can be obtained from the corresponding author upon reasonable request.

### Supporting Information

The Supporting Information is available free of charge at https://pubs.acs.org/doi/10.1021/acsami.5c05687.

Critical pigment volume concentration analysis (Note 1); additional SEM images of $BaSO_4$ paint (Figure S1); additional SEM images of $CaCO_3$ paint (Figure S2); additional SEM images of the hBN paint (Figure S3); additional SEM images of top and cross-sectional views of WBCPs (Figure S4); solar reflectance comparison between WBCPs and commercial paints as a function of thickness, and spectral reflectance comparison between WBCPs and commercial water-based white paints (Figure S5); estimated versus measured solar reflectance of WBCPs as a function of paint thickness (Figure S6); outdoor cooling performance (Figure S7); and cooling power analysis of WBCPs (Figure S8) (PDF)

## ■ AUTHOR INFORMATION


### Corresponding Author

**Xiulin Ruan** − *School of Mechanical Engineering, Purdue University, West Lafayette, Indiana 47907, United States; Flex lab and Birck Nanotechnology Center, Purdue University, West Lafayette, Indiana 47907, United States;* orcid.org/0000-0001-7611-7449; Email: ruan@purdue.edu

### Authors

**Abdulrahman K. Aljwirah** − *School of Mechanical Engineering, Purdue University, West Lafayette, Indiana 47907, United States; Flex lab, Purdue University, West Lafayette, Indiana 47907, United States; Department of Mechanical Engineering, Faculty of Engineering, University of Tabuk, Tabuk 71491, Saudi Arabia;* orcid.org/0009-0001-6214-5681

**Xiaojie Liu** − *School of Mechanical Engineering, Purdue University, West Lafayette, Indiana 47907, United States; Flex lab and James Tarpo Jr. and Margaret Tarpo Department of Chemistry, Purdue University, West Lafayette, Indiana 47907, United States*

**Orlando Rivera Gonzalez** − *School of Mechanical Engineering, Purdue University, West Lafayette, Indiana 47907, United States; Flex lab, Purdue University, West Lafayette, Indiana 47907, United States*

**Khalid Alhammadi** − *School of Mechanical Engineering, Purdue University, West Lafayette, Indiana 47907, United*




https://doi.org/10.1021/acsami.5c05687
ACS Appl. Mater. Interfaces 2025, 17, 32914−32927

*States; Flex lab, Purdue University, West Lafayette, Indiana 47907, United States; College of Engineering, King Saud University, Riyadh 11421, Saudi Arabia*

**Won-June Lee** − *James Tarpo Jr. and Margaret Tarpo Department of Chemistry, Purdue University, West Lafayette, Indiana 47907, United States;* orcid.org/0000-0001-8756-0956

**Ioanna Katsamba** − *School of Mechanical Engineering, Purdue University, West Lafayette, Indiana 47907, United States; Flex lab, Purdue University, West Lafayette, Indiana 47907, United States;* orcid.org/0000-0001-7296-152X

Complete contact information is available at: https://pubs.acs.org/10.1021/acsami.5c05687

### Author Contributions

[▽]X.R. is a lead contact. Conceptualization, X.R. and A.A.; methodology, X.R. and A.A.; investigation, A.A., X.L., O.R.G., K.A., W.-J.L., and I.K.; writing (original draft) A.A.; writing (review and editing), X.R., X.L., O.R.G., and K.A.; resources, X.R.; and supervision, X.R. The manuscript was written through the contributions of all authors. All authors have approved the final version of the manuscript.

### Notes

The authors declare the following competing financial interest(s): X.R., and A.A. are the inventors of a non-provisional international patent application (PCT/US2023/081605) filed on November 29, 2023.

## ■ ACKNOWLEDGMENTS

A.A. acknowledges support from the Saudi Arabian Cultural Mission and the University of Tabuk. X.R. and I.K. acknowledge partial support from the US National Science Foundation through award 2102645. X.L. acknowledges support from the Gilbreth Postdoctoral Fellowship from Purdue University. O.R.G. acknowledges the support from the US National Science Foundation Graduate Research Fellowship. K.A. acknowledges support from the Saudi Arabian Cultural Mission and King Saud University. W.-J.L. acknowledges the support from Ambilight Inc. under contract #4000187.02. The authors thank Dr. Jianguo Mei, Dr. Dudong Feng, Daniel William Carne, Andrea Lorena Felicelli, Emily Barber, and Sultan M AlNajdi for their invaluable assistance and discussions. Additionally, the authors acknowledge the generous support from EVONIK Industries and Innovative Chemical Technology (ITC), who supplied materials for this work.

## ■ REFERENCES

(1) Demirbas, A.; Hashem, A. A.; Bakhsh, A. A. The Cost Analysis of Electric Power Generation in Saudi Arabia. *Energy Sources, Part B* **2017**, *12* (6), 591−596.

(2) It gets hot in Saudi Arabia: 2800 h of sunshine at an average of 33.6 °C. Worlddata. https://www.worlddata.info/asia/saudi-arabia/climate.php (accessed November 01, 2024).

(3) Schmidt, J. Investment in air-conditioning needed to address future heat waves | PreventionWeb I. https://www.preventionweb.net/news/major-investment-air-conditioning-needed-address-future-heat-waves (accessed January 25, 2025).

(4) Catalanotti, S.; Cuomo, V.; Piro, G.; Ruggi, D.; Silvestrini, V.; Troise, G. The Radiative Cooling of Selective Surfaces. *Sol. Energy* **1975**, *17* (2), 83−89.

(5) Harrison, A. W.; Walton, M. R. Radiative Cooling of TiO2 White Paint. *Sol. Energy* **1978**, *20* (2), 185−188.

(6) Raman, A. P.; Anoma, M. A.; Zhu, L.; Rephaeli, E.; Fan, S. Passive Radiative Cooling below Ambient Air Temperature under Direct Sunlight. *Nature* **2014**, *515* (7528), 540−544.

(7) Kou, J.-l.; Jurado, Z.; Chen, Z.; Fan, S.; Minnich, A. J. Daytime Radiative Cooling Using Near-Black Infrared Emitters. *ACS Photonics* **2017**, *4* (3), 626−630.

(8) Tian, Y.; Shao, H.; Liu, X.; Chen, F.; Li, Y.; Tang, C.; Zheng, Y. Superhydrophobic and Recyclable Cellulose-Fiber-Based Composites for High-Efficiency Passive Radiative Cooling. *ACS Appl. Mater. Interfaces* **2021**, *13* (19), 22521−22530.

(9) Li, T.; Zhai, Y.; He, S.; Gan, W.; Wei, Z.; Heidarinejad, M.; Dalgo, D.; Mi, R.; Zhao, X.; Song, J.; Dai, J.; Chen, C.; Aili, A.; Vellore, A.; Martini, A.; Yang, R.; Srebric, J.; Yin, X.; Hu, L. A Radiative Cooling Structural Material. *Science* **2019**, *364* (6442), 760−763.

(10) Sethupathy, S.; Morales, G. M.; Gao, L.; Wang, H.; Yang, B.; Jiang, J.; Sun, J.; Zhu, D. Lignin Valorization: Status, Challenges and Opportunities. *Bioresour. Technol.* **2022**, *347*, No. 126696.

(11) Mandal, J.; Fu, Y.; Overvig, A. C.; Jia, M.; Sun, K.; Shi, N. N.; Zhou, H.; Xiao, X.; Yu, N.; Yang, Y. Hierarchically Porous Polymer Coatings for Highly Efficient Passive Daytime Radiative Cooling. *Science* **2018**, *362* (6412), 315−319.

(12) Huang, Z.; Ruan, X. Nanoparticle Embedded Double-Layer Coating for Daytime Radiative Cooling. *Int. J. Heat Mass Transfer* **2017**, *104*, 890−896.

(13) Li, X.; Peoples, J.; Huang, Z.; Zhao, Z.; Qiu, J.; Ruan, X. Full Daytime Sub-Ambient Radiative Cooling in Commercial-like Paints with High Figure of Merit. *Cell Rep. Phys. Sci.* **2020**, *1* (10), 100221.

(14) Li, X.; Peoples, J.; Yao, P.; Ruan, X. Ultrawhite $BaSO_4$ Paints and Films for Remarkable Daytime Subambient Radiative Cooling. *ACS Appl. Mater. Interfaces* **2021**, *13* (18), 21733−21739.

(15) Felicelli, A.; Katsamba, I.; Barrios, F.; Zhang, Y.; Guo, Z.; Peoples, J.; Chiu, G.; Ruan, X. Thin Layer Lightweight and Ultrawhite Hexagonal Boron Nitride Nanoporous Paints for Daytime Radiative Cooling. *Cell Rep. Phys. Sci.* **2022**, *3* (10), No. 101058.

(16) Hu, Z.-Y.; Chang, J.; Guo, F.-F.; Deng, H.-Y.; Pan, G.-T.; Li, B.-Y.; Zhang, Z.-L. The Effects of Dimethylformamide Exposure on Liver and Kidney Function in the Elderly Population. *Medicine* **2020**, *99* (27), No. e20749.

(17) Scailteur, V.; Lauwerys, R. R. Dimethylformamide (DMF) Hepatotoxicity. *Toxicology* **1987**, *43* (3), 231−238.

(18) Schieweck, A.; Bock, M.-C. Emissions from Low-VOC and Zero-VOC Paints − Valuable Alternatives to Conventional Formulations Also for Use in Sensitive Environments? *Build. Environ.* **2015**, *85*, 243−252.

(19) Lio, G. E.; Werlé, J.; Arduini, M.; Wiersma, D. S.; Manara, J.; Pattelli, L. Radiative Cooling Potential of a Water-Based Paint Formulation under Realistic Application Conditions. *ACS Appl. Opt. Mater.* **2024**, *2*, 2459−2468.

(20) Ju, H.; Lei, S.; Wang, F.; Long, H.; Yang, S.; Ou, J.; Amirfazli, A.; Baldelli, A. Low-Cost Waterborne Radiative Cooling Paint for Large Scale Production and Application in Buildings. *Colloids Surf., A* **2024**, *683*, No. 132962.

(21) Gong, Q.; Lu, L.; Chen, J.; Yin Lau, W.; Ho Cheung, K. A Novel Aqueous Scalable Eco-Friendly Paint for Passive Daytime Radiative Cooling in Sub-Tropical Climates. *Sol. Energy* **2023**, *255*, 236−242.

(22) Yoon, J.; Lee, J.; Kim, H.; Kim, J.; Jin, H.-J. Polymeric Binder Design for Sustainable Lithium-Ion Battery Chemistry. *Polymers* **2024**, *16* (2), No. 254.

(23) Aguirre, M.; Ballard, N.; Gonzalez, E.; Hamzehlou, S.; Sardon, H.; Calderon, M.; Paulis, M.; Tomovska, R.; Dupin, D.; Bean, R. H.; Long, T. E.; Leiza, J. R.; Asua, J. M. Polymer Colloids: Current Challenges, Emerging Applications, and New Developments. *Macromolecules* **2023**, *56* (7), 2579−2607.

(24) Arkles, B. Hydrophobicity, Hydrophilicity and Silanes. *Paint Coat. Ind.* **2006**, *22* (10), 114−135.

(25) *Paint and Surface Coatings: Theory and Practice*, 2nd ed.; Lambourne, R.; Strivens, T. A., Eds.; William Andrew Pub: Norwich, NY, 1999.
(26) Li, Y.; Zhang, X.; Zhang, T.; Chen, Y.; Zhang, S.; Yu, D.; Wang, W. Radiative Cooling Materials Prepared by SiO2 Aerogel microspheres@PVDF-HFP Nanofilm for Building Cooling and Thermal Insulation. *Ceram. Int.* **2024**, *50* (22), 48031−48040.
(27) Díaz-Lobo, A.; Martin-Gonzalez, M.; Song, Q.; Morales-Sabio, Á.; Retsch, M.; Manzano, C. V. Metallic Coatings Boost the Cooling Power of Nanoporous Alumina. *ACS Appl. Eng. Mater.* **2024**, *2* (8), 2069−2079.
(28) Zhang, Y.; Tan, X.; Qi, G.; Yang, X.; Hu, D.; Fyffe, P.; Chen, X. Effective Radiative Cooling with ZrO2/PDMS Reflective Coating. *Sol. Energy Mater. Sol. Cells* **2021**, *229*, No. 111129.
(29) Ruan, X.; Aljwirah, A. Water-Based Radiative Cooling Paint Mixtures and Single-Layer Paints for Passive Radiative Cooling. WO Patent WO2024118777A1. (accessed February 21, 2025).
(30) Menzies, J.; Wilcox, A.; Casteel, K.; McDonough, K. Water Soluble Polymer Biodegradation Evaluation Using Standard and Experimental Methods. *Sci. Total Environ.* **2023**, *858*, No. 160006.
(31) Mohammed, M. I.; El-Sayed, F. PEG's Impact as a Plasticizer on the PVA Polymer's Structural, Thermal, Mechanical, Optical, and Dielectric Characteristics. *Opt. Quantum Electron.* **2023**, *55* (13), No. 1141.
(32) Nasatto, P.; Pignon, F.; Silveira, J.; Duarte, M.; Noseda, M.; Rinaudo, M. Methylcellulose, a Cellulose Derivative with Original Physical Properties and Extended Applications. *Polymers* **2015**, *7* (5), 777−803.
(33) Voogt, B.; Huinink, H. P.; Erich, S. J. F.; Scheerder, J.; Venema, P.; Keddie, J. L.; Adan, O. C. G. Film Formation of High Tg Latex Using Hydroplasticization: Explanations from NMR Relaxometry. *Langmuir* **2019**, *35* (38), 12418−12427.
(34) Pouget, E.; Tonnar, J.; Lucas, P.; Lacroix-Desmazes, P.; Ganachaud, F.; Boutevin, B. Well-Architectured Poly-(Dimethylsiloxane)-Containing Copolymers Obtained by Radical Chemistry. *Chem. Rev.* **2010**, *110* (3), 1233−1277.
(35) Diebold, M. P. *Application of Light Scattering to Coatings: A User's Guide*; Springer, 2014; ref 30.
(36) Sands, S. Pigment Volume Concentration and its Role in Color. Just Paint. https://justpaint.org/pigment-volume-concentration-and-its-role-in-color/. (accessed June 06, 2023).
(37) Müller, B.; Poth, U. *Coatings Formulation: An International Textbook*; Vincentz Network, 2019.
(38) Zhu, F. L.; Feng, Q. Q. Pore Feature Size Influence on Optical-Infrared Properties of Porous Polyamide Film. *Mater. Lett.* **2023**, *346*, No. 134525.
(39) Standard Test Method for Oil Absorption of Pigments by Spatula Rub-out. https://www.astm.org/d0281-12r21.html (accessed October 14, 2024).
(40) Koleske, J. V.; Glancy, C. W. Oil Absorption of Pigments. In *Paint and Coating Testing Manual: 15th. ed. of the Gardner-Sward Handbook*; Koleske, J. V., Ed.; ASTM International: West Conshohocken, PA, 2012; pp 300−311.
(41) Atiganyanun, S.; Plumley, J. B.; Han, S. J.; Hsu, K.; Cytrynbaum, J.; Peng, T. L.; Han, S. M.; Han, S. E. Effective Radiative Cooling by Paint-Format Microsphere-Based Photonic Random Media. *ACS Photonics* **2018**, *5* (4), 1181−1187.
(42) Atiganyanun, S.; Kumnorkaew, P. Effects of Pigment Volume Concentration on Radiative Cooling Properties of Acrylic-Based Paints with Calcium Carbonate and Hollow Silicon Dioxide Microparticles. *Int. J. Sustainable Energy* **2023**, *42* (1), 612−626.
(43) Aguirre-Ramírez, M.; Silva-Jiménez, H.; Banat, I. M.; De Rienzo, M. A. D. Surfactants: Physicochemical Interactions with Biological Macromolecules. *Biotechnol. Lett.* **2021**, *43* (3), 523−535.
(44) Patterson, R. E. Influence of Silica Properties on Performance of Antifoams in Pulp and Paper Applications 2. In-Situ Hydrophobing. *Colloids Surf., A* **1993**, *74* (1), 115−126.
(45) Standard Test Method for Fineness of Dispersion of Pigment-Vehicle Systems by Hegman-Type Gage. https://www.astm.org/d1210-05r22.html (accessed October 12, 2024).
(46) Röhrl, M.; Mettke, J. H.; Rosenfeldt, S.; Schmalz, H.; Mansfeld, U.; Timmins, R. L.; Habel, C.; Breu, J.; Durst, F. Shear Orientation of Nematic Phases of Clay Nanosheets: Processing of Barrier Coatings. *J. Coat. Technol. Res.* **2022**, *19* (2), 487−495.
(47) Carne, D.; Peoples, J.; Arentz, F.; Ruan, X. True Benefits of Multiple Nanoparticle Sizes in Radiative Cooling Paints Identified with Machine Learning. *Int. J. Heat Mass Transfer* **2024**, *222*, No. 125209.
(48) Mazrouei-Sebdani, Z.; Khoddami, A. Alkaline Hydrolysis: A Facile Method to Manufacture Superhydrophobic Polyester Fabric by Fluorocarbon Coating. *Prog. Org. Coat.* **2011**, *72* (4), 638−646.
(49) Handajani, U.; Widati, A. A.; Yusbainika, I. Preparation Hydrophobic Fabric Coated by TiO 2 and Hexadecyltrimethoxysilane. *IOP Conf. Ser.: Earth Environ. Sci.* **2018**, *217*, No. 012011.
(50) Hays, H. L.; Mathew, D.; Chapman, J. Fluorides and Fluorocarbons Toxicity. In *StatPearls*; StatPearls Publishing: Treasure Island (FL), 2025.
(51) Owen, M. J. Silicone Hydrophobicity and Oleophilicity. *Silicon* **2017**, *9* (5), 651−655.
(52) Yang, C.; Tartaglino, U.; Persson, B. N. J. Influence of Surface Roughness on Superhydrophobicity. *Phys. Rev. Lett.* **2006**, *97* (11), No. 116103.
(53) Parrack, B. Calculations. https://www.aqmd.gov/home/rules-compliance/compliance/vocs/calculations (accessed July 07, 2024).
(54) Rule 1113 Table of Standards. https://www.aqmd.gov/home/rules-compliance/compliance/vocs/architectural-coatings/tos (accessed June 13, 2024).
(55) NEWS ALERT: Are You Confused About VOCs? Here's How to Navigate Cortec Coatings - Cortec Coatings_. www.CortecVCI.comhttps://www.corteccoatings.com/2023/03/10/news-alert-are-you-confused-about-vocs-heres-how-to-navigate-cortec-coatings/ (accessed January 23, 2025).
(56) Pianoforte, K. Difference between VOC compliant and low VOC adhesives and sealants. https://www.coatingsworld.com/issues/2020-04-01/view_features/low-and-zero-voc-coatings-743114/.
(57) Peoples, J.; Li, X.; Lv, Y.; Qiu, J.; Huang, Z.; Ruan, X. A Strategy of Hierarchical Particle Sizes in Nanoparticle Composite for Enhancing Solar Reflection. *Int. J. Heat Mass Transfer* **2019**, *131*, 487−494.
(58) Fitzsimons, B.; Parry, T. Coating Failures and Defects. In *Protective Organic Coatings*; Tator, K. B., Ed.; ASM International, 2015; pp 502−512.
(59) Moradi, N.; Kandi, S. G.; Yahyaei, H. A New Approach for Detecting and Grading Blistering Defect of Coatings Using a Machine Vision System. *Measurement* **2022**, *203*, No. 111954.
(60) D20 Committee. Test Method for Water Absorption of Plastics. DOI: 10.1520/D0570-22.
(61) Tocháček, J.; Vrátníčková, Z. Polymer Life-Time Prediction: The Role of Temperature in UV Accelerated Ageing of Polypropylene and Its Copolymers. *Polym. Test.* **2014**, *36*, 82−87.
(62) Frigione, M. Assessment of the Ageing and Durability of Polymers. *Polymers* **2022**, *14* (10), No. 1934.
(63) Mecklenburg, M. F. Methods and Materials and the Durability of Canvas Paintings: A Preface to the Topical Collection Failure Mechanisms in Picasso's Paintings. *SN Appl. Sci.* **2020**, *2* (12), No. 2182.
(64) ISO 16474-1. 2013 https://www.iso.org/standard/56803.html (accessed October 13, 2024).
(65) Hamedi, R. F. Evaluation of the Color Stability of Methyl Methacrylate and Nylon Base Polymer. *J. Dent.* **2017**, *18* (2), 136−142.
(66) González-Cabrera, M.; Domínguez-Vidal, A.; Ayora-Cañada, M. J. Monitoring UV-Accelerated Alteration Processes of Paintings by Means of Hyperspectral Micro-FTIR Imaging and Chemometrics. *Spectrochim. Acta, Part A* **2021**, *253*, No. 119568.

(67) Standard Test Method for Abrasion Resistance of Organic Coatings by the Taber Abraser. https://www.astm.org/d4060-19.html (accessed October 13, 2024).
(68) Hegemann, D. Plasma Polymer Deposition and Coatings on Polymers. In *Comprehensive Materials Processing*; Elsevier, 2014; pp 201−228.
(69) Standard Test Methods for Rating Adhesion by Tape Test. https://www.astm.org/d3359-23.html (accessed November 17, 2024).
(70) Das, A.; Mahanwar, P. A Brief Discussion on Advances in Polyurethane Applications. *Adv. Ind. Eng. Polym. Res.* **2020**, *3* (3), 93−101.


https://doi.org/10.1021/acsami.5c05687
*ACS Appl. Mater. Interfaces* 2025, 17, 32914−32927